Res Chem Intermed
DOI 10.1007/s11164-015-2369-7

Scanning electrochemical microscopy for the investigation of corrosion inhibition of triazino-benzimidazole-2-thiones in hydrochloric acid solution

N. Esmaeili[1] · J. Neshati[1] · I. Yavari[2]

Received: 16 June 2015 / Accepted: 19 November 2015

Abstract Aryl-triazino-benzimidazole-2-thiones were synthesized via three-component reaction between ammonium thiocyanate, benzoyl chlorides, and 2-aminobenzimidazole in acetone. The structure of the products was confirmed by NMR, FT-IR, and mass spectrometer. The corrosion behaviors of these compounds on carbon steel in 2 M HCl solution were investigated by scanning electrochemical microscopy, operated in the substrate-generation/tip-collection mode using Fe^{2+}/Fe^{3+} redox couple as redox mediator. The tip current values and local ferrous ion concentrations were obtained. The inhibition efficiency of the inhibitors was investigated by weight loss measurements. When the inhibition efficiency was more than 85 %, scanning electrochemical microscopy and weight loss measurements were in good agreement.

Keywords Scanning electrochemical microscopy · Benzoimidazole · Corrosion inhibition

Introduction

The coupling of scanning probe techniques with electrochemistry were performed by Bard in 1989 [1]. Scanning electrochemical microscopy (SECM) has become a powerful technique in many areas of fundamental electrochemical research, due to its high spatial resolution and sensitivity. This technique consists of a mobile ultramicroelectrode (UME), which has developed into a versatile tool for the

✉ J. Neshati
neshatij@ripi.ir

[1] Industrial Protection Division, Research Institute of Petroleum Industry, P.O. Box 14665-137, Tehran, Iran

[2] Department of Chemistry, Tarbiat Modares University, P.O. Box 14115-175, Tehran, Iran

Published online: 29 December 2015

investigation of the topography and redox activity of solid–liquid, liquid–liquid, and liquid–gas interfaces [2, 3]. Information about reactions that occur in the solution space between the tip and sample can also be obtained, which has facilitated the use of this technique in applications beyond the solid/liquid interface [4–6]. SECM has been used in measuring, characterizing, and evaluating corroding systems [7]. Localized corrosion processes and electrochemical activity distributions on surfaces can thus be investigated in real time with high spatial resolution. SECM has been used to study corrosion and the localized corrosion phenomena at surfaces [8–12]. The substrate generation–tip collection (SG/TC) mode in SECM has been usually exploited for such purposes [13–15]. In the SG/TC mode, a redox-active species is generated at the sample and is amperometrically detected at the UME. Local fluxes of ferrous ions at steel surfaces have been monitored by oxidation of Fe^{2+} ions at the tip [16–21].

In this work, four aryl-triazino-benzimidazole-2-thiones (**1a**–**1d**) were prepared via multicomponent reactions [9, 22–27] from thiocynate, benzoyl chlorides, and 2-aminobenzimidazole. The applicability of SECM was investigated to characterize the inhibiting effect of these compounds against the corrosion of carbon steel in 2 M HCl solution. Direct SECM evidence for the corrosion process was obtained through the amperometric measurement of Fe^{2+} ions as the dissolution of the carbon steel proceeds in acidic conditions. The ferrous ion concentrations were calculated by using tip current (i_{tip}). In addition, the inhibition efficiency of the inhibitors was studied using weight loss measurements. The adsorption mechanism was investigated by calculating isotherm equations.

Materials and instruments

The reagents and solvents used in this study were obtained from Merck and used without further purification. Melting points were recorded on a Buchi 535 apparatus. IR spectra, Shimadzu IR-460 spectrometer; ^{1}H- and ^{13}C-NMR spectra, Bruker DRX-300 Avance; EI-MS (70 eV): Finnigan MAT-8430 mass spectrometer in *m/z*; SECM, Uniscan model 370, UK; potentiostat/Galvanostat, Zahner model MeX6, Germany; were used.

General procedure for the preparation of aryl-triazino-benzimidazole-2-thiones

Aryloylisothiocyanates 3 were prepared from ammonium thiocyanate (1.52 g, 20 mmol) and benzoyl chlorides (20 mmol) in acetone (30 mL) at room temperature. Then, 2-amino-benzoamidazole (2.66 g, 20 mmol) was added. The reaction mixture was refluxed for 2 h, solvent removed and the residue was purified by recrystallization from EtOH to give product **1** (Fig. 1). The structures of products

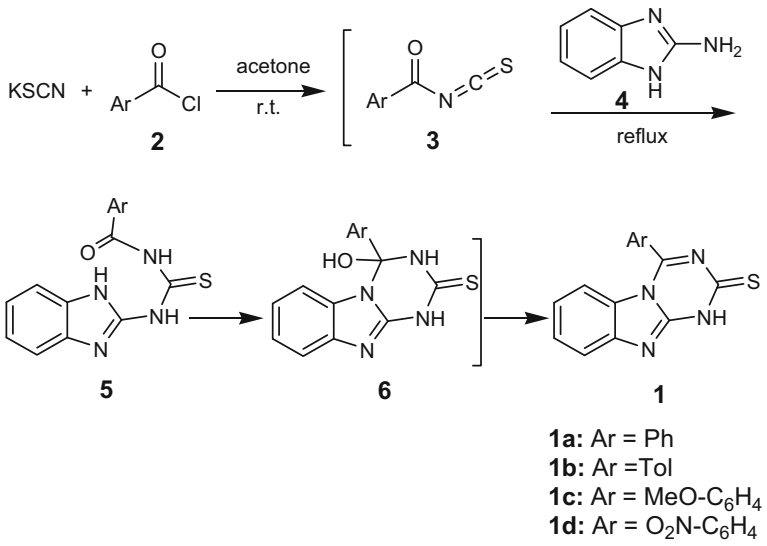

Fig. 1 Synthesis of aryl-triazino-benzimidazole-2-thiones **1a–1d**

1a–1d were deduced from their IR, ^{1}H- and ^{13}C-NMR spectroscopy, and mass spectrometry.

4-Phenyl[1, 3, 5]triazino[1,2-a]benzimidazole-2(1H)-thione (**1a**) Yellow powder; yield: (75 %); IR (KBr): 3434 (NH), 3100, 1622 1474; ^{1}H-NMR (300 MHz, DMSO-*d*6): 9.40 (s, 1H); 8.42 (d, $^{3}J = 7.3$ Hz, 2H); 7.40-7.60 (m, 7 H); ^{13}C-NMR (70 MHz, DMSO-*d*6): 178.7 (C=S); 150.4 (C); 142.0 (C); 134.3 (C); 132.0 (CH); 128.4 (2 CH); 128.2 (2 CH), 127.1 (CH); 126.6 (C); 122.1 (CH); 116.9 (2 CH); 112.1(C). MS: *m/z* (%) = 278 (M^{+}, 100), 245 (5), 219 (56.7), 192 (5), 175 (53.3), 104 (6.7), 90 (8.3), 77 (10).

4-(4-Methylphenyl)[1, 3, 5]triazino[1,2-a]benzimidazole-2(1H)-thione (**1b**) Yellow powder; yield: (81 %); IR (KBr): 3356 (NH), 3063, 1658; 1256 (C=S); ^{1}H-NMR (300 MHz, DMSO-*d*6): 9.35 (s, 1H); 8.01 (d, $^{3}J = 8.2$ Hz, 2 H); 7.21 (d, $^{3}J = 8.2$ Hz, 2 H); 7.17–7.11 (m, 4 CH); ^{13}C-NMR (70 MHz, DMSO-*d*6): 177.1 (C=S); 167.6 (C); 162.1 (C) 155.4 (C); 148.1 (C); 142.4 (CH); 134.4 (C); 131.0 (CH); 129.4 (C); 129.0 (2 CH); 128.3 (2 CH); 121.61 (CH); 113.5 (CH); 21.1 (Me); MS: *m/z* (%) = 292 (M^{+}, 5), 251 (52), 223 (32), 194 (10), 105 (14), 119 (100), 91 (65), 65 (30).

(4-Methoxyphenyl)[1, 3, 5]triazino[1,2-a]benzimidazole-2(1H)-thione (**1c**) Yellow powder; yield: (83 %); IR (KBr): 3421 (NH), 3074, 2837; 1692, 1260 (C=S); ^{1}H-NMR (300 MHz, DMSO-*d*6): 12.3 (s, 1H); 8.15 (d, $^{3}J = 8.1$ Hz, 2 H); 7.46 (d, $^{3}J = 7.9$ Hz, 2 H); 7.11–6.99 (m, 4 H); 3.82 (s, 3 H); ^{13}C-NMR (70 MHz, DMSO-*d*6): 182.2 (C=S); 166.9 (C); 163.1 (C); 162.5 (C); 148.4 (C); 135.0 (C); 130.9 (CH); 130.3 (2 CH), 125.9 (CH); 124.8 (C); 121.4 (CH); 113.7 (2CH); 113.6 (CH); 55.5 (MeO). MS: *m/z* (%) = 308 (M^{+}, 31), 267 (78), 239 (20), 135 (100), 92 (15), 77 (18).

4-(4-Nitrophenyl)[1, 3, 5]triazino[1,2-a]benzimidazole-2(1H)-thione (**1d**) Yellow powder; yield: (85 %); IR (KBr): 3353, (NH); 1680; 1554, 1339 (NO_2); 1159 (C=S); ^{1}H-NMR (300 MHz, DMSO-*d*6): 9.68 (s, 1 H); 8.54 (d, $^3J = 8.7$ Hz, 2 H); 8.28 (d, $^3J = 9.18$ Hz, 2 H); 8.13 (d, $^3J = 8.7$ Hz, 1 H); 7.61 (d, $^3J = 8.8$ Hz, 1 H); 7.53 (t, $^3J = 7.3$ Hz, 1 H); 7.44 (t, $^3J = 7.4$ Hz, 1 H); ^{13}C-NMR (70 MHz, DMSO-*d*6): 189.3 (C=S); 169.6 (C); 156.9 (C); 149.8 (C); 145.4 (C); 140.9 (C); 130.7 (2 CH), 130.2 (CH), 128.8 (CH); 124.8 (CH); 123.7 (2 CH); 113.51 (CH); MS: *m/z* (%) = 323 (M^+, 53), 282 (98), 254 (51), 160(53), 150 (100), 104 (41), 92 (24), 76 (35).

Electrochemical measurements

SECM photographs were obtained from the carbon steel surface by using a scanning electrochemical microscope. The electrodes were a 25 μm platinum UME tip, an Ag/AgCl/KCl (saturated) reference electrode, sample electrode (carbon steel), and a platinum counter electrode, all set up in a cell made of poly(tetrafluoroethene). Scans were conducted parallel to the sample surface in an area of 500 μm × 500 μm in *X* and *Y* directions. Scan rate was 10 μm s^{-1}. The measurements were performed with the UME tip at a height of 20 μm over the specimen surface. Fe^{2+}/Fe^{3+} redox couple was used as electrochemical mediator at the tip. The gap (20 μm) between the UME and carbon steel was measured using the scaled video camera system attached to the SECM. The potential of the tip was held at +0.6 V versus the reference electrode. The carbon steel samples with composition 0.19 % C, 0.4 % Mn, 0.04 % P, 0.005 % S, and Fe for the balance were used for weight loss studies of inhibitors.

Results and discussion

SECM experiments

The presence iron ions at the carbon steel surface under the UME tip was examined by SECM. The tip distance over the sample was determined by approach curves. These curves were drawn when the tip was moved towards the surface in a controlled motion on the *Z* axis [28]. Approach curve in Fig. 2 shows the concentration profile of Fe^{2+} ions as a function of the distance from the carbon steel surface in 2 M HCl. Approach curve was measured at the open-circuit potential. According to Fig. 2, at a distance of <20 μm, the current reaches the current limit. Therefore, the distance between tip and sample surface should be set <20 μm.

Corrosion occurs when the carbon steel is exposed to the acidic solution resulting in the release of Fe^{2+} ions in the anodic half-cell reaction based on Eq. (1). The ferrous ions are detected at the UME through their oxidation to Fe^{3+} ions by setting the tip potential at +0.60 V based on Eq. (2), as shown in Fig. 3.

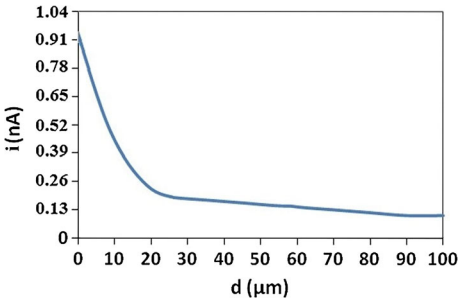

Fig. 2 SECM approach curve with tip potential +0.60 V versus Ag/AgCl/KCl (saturated) of the carbon steel surface measured in 2 M HCl solution at the open-circuit potential

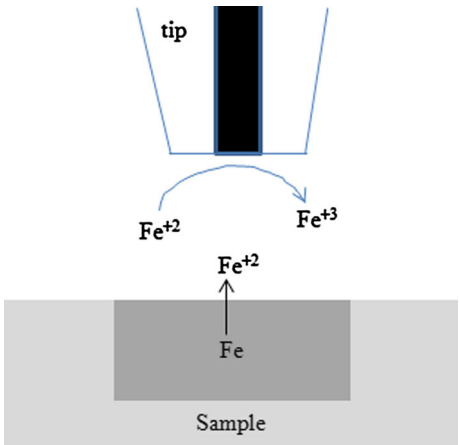

Fig. 3 Schematic representation of the SECM tip operating at +0.6 V

$$\text{Dissolution reaction on Sample: Fe} \rightarrow \text{Fe}^{2+} + 2\text{e}^{-} \quad (1)$$

$$\text{UME: Fe}^{2+} \rightarrow \text{Fe}^{3+} + \text{e}^{-} \quad (2)$$

Figure 4 shows a cyclic voltammogram measured at the UME tip in a 2 M HCl solution at the scan rate of 0.05 V s^{-1}. It depicts the electrochemical reactions associated with the dissolved Fe(II) ions in the electrolyte. The voltammetric wave corresponds to the Fe(II)/Fe(III) electrode reaction as shown in Eq. (2). By setting the tip potential to +0.60 V versus Ag/AgCl/KCl (sat.), the oxidation of the Fe(II) species dissolved in the electrolyte can be detected through their oxidation to Fe(III) at the UME. Since no Fe(II) species were originally present in the electrolytic phase, they can only originate from corrosion processes at the carbon steel metal directly exposed to the 2 M HCl solution.

The cathodic process consumes H^{+} and dissolved oxygen from the solution phase. In acidic media, species are consumed or generated on sample through possible reactions which can be summarized by the following equations [4, 13]. At low pH and oxygen-poor solutions, it may be assumed that the cathodic reaction is the reduction of protons (6).

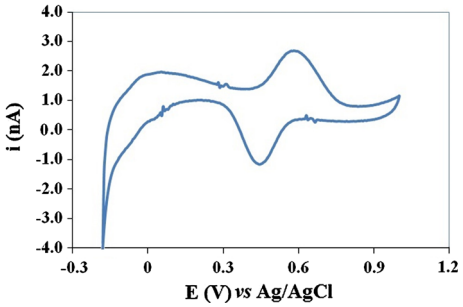

Fig. 4 Cyclic voltammogram measured at the SECM-tip in 2 M HCl of carbon steel sample with scan rate of 0.05 V s^{-1}

$$O_2 + 4H^+ + 4e^- \rightarrow 2H_2O \quad (3)$$

$$O_2 + 2H^+ + 2e^- \rightarrow H_2O_2 \quad (4)$$

$$2H_2O_2 \rightarrow 2H_2O + O_2 \text{ (decomposition reaction)} \quad (5)$$

$$2H^+ + 2e^- \rightarrow H_2 \quad (6)$$

The release of metal ions at sample surface and the consumption of Fe^{2+} at the tip can be monitored during operation in the generator–collector mode [29, 30]. Therefore, changes in the local concentration of ferrous ions were recorded by scanning the microelectrode over the sample when the proper potential value (+0.6) was set at the tip.

SECM plots in Fig. 5 were used to study the film formation of aryl-triazino-benzimidazole-2-thiones **1a**–**1d** on the carbon steel in 2 M HCl solution. Based on Fig. 5a in the absence of an inhibitor, the current fluctuations were induced by anodic dissolution occurring on the carbon steel sample surface. As shown in Fig. 5b, the local defects in the corrosion of carbon steel in the presence **1a** inhibitor are considered the potential precursor sites for localized corrosion, when thin surface films are formed during the adsorption of corrosion inhibitors on metals. The resulting SECM maps showed that maximum of current density was 1.7×10^{-5} A (17 μA) in blank solution. The current maximum observed for **1a**–**1d** inhibitors were 2.1×10^{-7}, 3.8×10^{-8}, 1.7×10^{-8} , and 2.3×10^{-7} A, respectively. The corrosion inhibition were calculated based on the mean corrosion currents which are represented and replaced by tip currents characterizing the oxidation of Fe(II) species from corrosion reaction of carbon steel (Table 1). The inhibition efficiency (IE_{SECM}) at each inhibitor concentration was calculated from the value of the maximum current using the Eq. (7):

$$IE_{SECM}\% = \left(\frac{i_{tip(max)} - i'_{tip(max)}}{i_{tip(max)}} \right) \times 100 \quad (7)$$

where $i_{tip(max)}$ and $i'_{tip(max)}$ are the maximum current density of the tip in the absence and presence of the inhibitor, respectively.

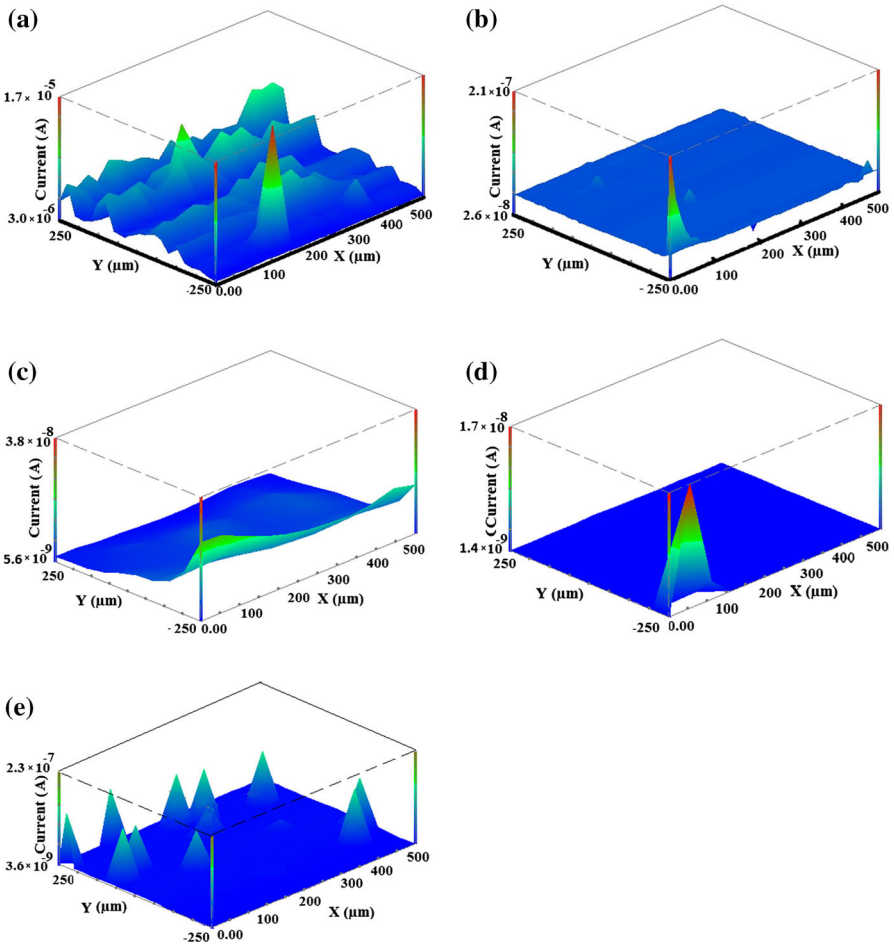

Fig. 5 Images created by SECM measurements on a carbon steel sample in 100 mg L^{-1} of inhibitor in 2 M HCl solution. *a* Blank, *b* **1a**, *c* **1b**, *d* **1c**, *e* **1d**. Tip–substrate distance: 20 µm. Tip potential: +0.6 V versus Ag/AgCl/KCl (saturated) reference electrode. The figures represent an area of 500 µm × 500 µm in *X* and *Y* directions

Based on Eq. (8), the values given in Table 1 indicate an estimate of the local ferrous ion concentration obtained from the steady-state current at the SECM tip [13].

$$i_{\text{tip}} = 4nr_{\text{o}}FDC, \tag{8}$$

where n ($n = 1$) is the number of electrons transferred during the redox reaction, r_{o} is the radius of the UME, F is the Faraday constant (96,485 C mol^{-1}), C is the local ferrous volume concentration, and D is the diffusion coefficient of the redox species. The diffusion coefficient of Fe^{2+} in 2 M HCl solution ($D = 3.3 \times 10^{-6}$ cm^2 s^{-1}) was calculated by using the Randles–Sevcik equation. This steady-state current is

Table 1 The tip currents, local ferrous ion concentrations and IE% of compounds **1a–1d** in 2 M HCl on the carbon steel at the different concentration

Inhibitor	C (mg L^{-1})	i_{tip} (A)	$C_{Fe(II)}$ (mM)	IE% From SECM	IE% From weight loss
Blank	–	1.0×10^{-5}	3.14	–	–
1a	25	4.02×10^{-6}	1.26	59.8	44.4
	50	1.21×10^{-6}	3.80×10^{-1}	87.9	76.9
	75	4.85×10^{-7}	1.52×10^{-1}	95.1	86.5
	100	1.18×10^{-7}	3.71×10^{-2}	99.8	90.2
1b	25	2.79×10^{-6}	8.76×10^{-1}	72.1	45.6
	50	4.90×10^{-7}	1.54×10^{-1}	95.0	80.6
	75	1.3×10^{-7}	4.08×10^{-2}	98.7	89.8
	100	2.46×10^{-8}	7.73×10^{-3}	99.8	93.5
1c	25	9.8×10^{-7}	3.08×10^{-1}	90.2	63.0
	50	4.25×10^{-7}	1.33×10^{-1}	95.7	82.1
	75	1.45×10^{-8}	4.55×10^{-3}	99.8	91.8
	100	9.8×10^{-9}	3.08×10^{-3}	99.9	95.4
1d	25	2.35×10^{-6}	7.38×10^{-1}	76.5	36.6
	50	8.60×10^{-7}	2.70×10^{-1}	91.4	73.8
	75	4.80×10^{-7}	1.51×10^{-1}	95.2	84.7
	100	1.17×10^{-7}	3.67×10^{-2}	98.7	89.0

explained with the diffusion layer being hemispherical in shape and extending out into the solution. The amount of Fe^{+2} species diffusing to the carbon steel surface is defined by the volume with this expanding hemisphere, rather than a plane projecting into the solution as for a planar electrode. The current at a small disk also reaches steady state in a fraction of a second. These characteristics show that a UME used as a scanning tip and moving in a solution can be treated as a steady-state system. In addition, the small currents that characterize most experiments with UME tips, resistive drops in the solution during the passage of current are generally negligible [31].

Table 1 shows the tip currents, local ferrous ion concentrations and IE% of compounds **1a–1d** at difference concentrations in 2 M HCl. The local concentration of Fe^{2+} were observed 3.2 mM at 20 μm from the surface of carbon steel in the absence of inhibitors. In the presence of inhibitors **1a–1d,** the ferrous ion concentration and tip current reduced. Increase in inhibitors concentration up to 100 mg L^{-1} caused iron ion concentrations and tip currents decreased (Table 1). The compound **1a** decreased the extent of acidic dissolution for the carbon steel, but the current fluctuations appeared on the sample surface (Fig. 5b). The local ferrous ion concentration and i_{tip} for compound **1a** were 0.039 mM and 2.1×10^{-7} A, respectively.

The adsorption of **1b–c** molecules on the carbon steel surface is responsible for reduction of corrosion current and formation of a uniform adsorption film (Fig. 5c-d). The corrosion current was decreased by the compound **1e**, but local

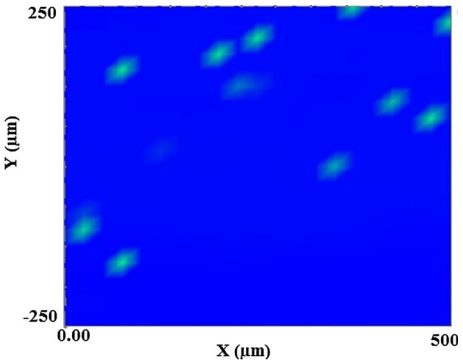

Fig. 6 SECM contour plot of carbon steel in 100 mg L^{-1} of inhibitor **1e** in 2 M HCl. $E_{tip} = +0.60$ V, E_{sample} = OCP, SECM Pt tip radius: 25 μm. Scan at constant height near the sample (20 μm)

defects appeared on the carbon steel surface (Fig. 5e). The contour plot in Fig. 6 has been shown as a typical SECM scan of compound **1e** over carbon steel at a constant height of about 20 μm, as obtained from approach curve. The contour plot clearly shows a localized production of ferrous ions above the defect of carbon steel. Based on IE_{SECM} calculated from Eq. (7) the performance of inhibitors was reduced in the following order: compound **1c** > compound **1b** > compound **1a** > compound **1d**.

All the compounds exhibited more than 98 % anticorrosion activity at the concentration of 100 mg L^{-1}. These compounds have several functional adsorption centers such as C=S groups, O and/or N heteroatoms, and aromatic rings. The adsorption of the examined inhibitors can occur by formation of links between the *d*-orbital of iron atoms and the lone pairs present on the N, O, and S atoms, as well as the π-bonds of the aromatic ring. The difference in the protective action of the aryl-triazino-benzimidazole-2-thiones may be explained by functional groups on the aromatic ring. Among the aryl-triazino-benzimidazole-2-thiones investigated in this study, **1c** had the best performance. This can be attributed to the electron-donating methoxy group. The presence of methoxy group enhances the possible interaction between the π-electrons with the vacant *d*-orbitals of iron atoms. Although the nitro group atom is electron-withdrawing, the presence of two oxygen atoms in its structure increases the corrosion inhibition.

Weight loss measurements

The weight loss experiments were carried out in 2 M HCl solutions for a duration of 6 h based on ASTM G31-2004. The samples were immersed in triplicate, and an average corrosion rate was calculated. The inhibition efficiency (IE) at each inhibitor concentration was calculated from the value of weight loss using the Eq. (9):

$$IE\% = \left(\frac{W_{uninh} - W_{inh}}{W_{uninh}}\right) \times 100 \tag{9}$$

where W_{inh} and W_{uninh} are the weight loss of the metal in presence and absence of the inhibitor, respectively. The results are listed in Table 1. It is obvious that the IE increases with increasing inhibitor concentration. According to Table 1, at

100 mg L^{-1} of inhibitors, the IE increases up to more than 89 %, which can be caused by the formation of a protective film on carbon steel surface. The electron-donating groups (methyl and methoxy) of the benzene ring in para position increased inhibition efficiency. The IE of the investigated inhibitors decreased in the following order: compound **1c** > compound **1b** > compound **1a** > compound **1d**. The IE obtained from SECM showed good agreement with those obtained from weight loss experiments. According to Table 1, it can be deduced that when inhibition efficiency was over 85 %, the amount the SECM methodology obtained was more than the weight loss method, and the difference of the two methods was about 10 %. The difference in results may be because the measurements of current at a small disk (UME) are done in a fraction of a second, while in the weight loss method, the average of corrosion is calculated. The corrosion current at the moment can be more or less than the average rate of corrosion.

Adsorption isotherms

Adsorption isotherms were used for the study of adsorption ability of aryl-triazino-benzimidazole-2-thiones **1a–1d** on the carbon steel in 2 M HCl solutions. In order to obtain the isotherm, the linear relation between degree of surface coverage and inhibitor concentration (C_{inh}) must be found. Surface coverage (θ) was determined from weight loss measurements according to Eq. (10):

$$\theta = \frac{IE\%}{100} \tag{10}$$

where IE is the inhibition efficiency from weight loss measurements.

Adsorption isotherms including Langmuir, Temkin, Frumkin, and Flory–Huggins were fitted for aryl-triazino-benzimidazole-2-thiones **1a–1d**. The best fit was obtained with the Langmuir isotherm (Fig. 7). According to this isotherm [32],

$$\frac{C_{inh}}{\theta} = C_{inh} + \frac{1}{K_{ads}} \tag{11}$$

where, C_{inh} is the inhibitor concentration, K_{ads} is the adsorption equilibrium constant, and θ is surface coverage given by Eq. (10). The constant of an adsorption,

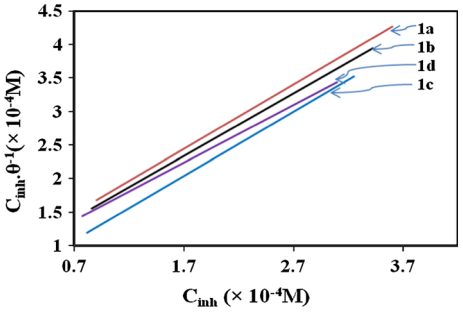

Fig. 7 Longmuir adsorption plots for carbon steel in 2 M HCl containing inhibitors of **1a–1d**

Table 2 The values of K_{ads} and ΔG°_{ads} of **1a**–**1d** for carbon steel in 2 M HCl in 298 k

Inhibitor	K_{ads} (10^4 M^{-1})	ΔG°_{ads} (kJ mol^{-1})
1a	1.22	−33.27
1b	1.31	−33.44
1c	2.42	−34.96
1d	1.29	−33.40

K_{ads}, is related to the standard free energy of adsorption, ΔG°_{ads}, with the following Eq. (12);

$$K_{ads} = \left(\frac{1}{55.55}\right) \exp\left(\frac{-\Delta G^{\circ}_{ads}}{RT}\right) \tag{12}$$

where, R is the universal gas constant and T is the absolute temperature.

Adsorption isotherm provides information on the adsorption process such as surface coverage, adsorption equilibrium constant, and information on the interaction between the organic compound and electrode surface. The negative values of ΔG°_{ads} in Table 2 indicate that adsorption of the inhibitors **1a**–**1d** on the carbon steel surface is spontaneous. It is well known that values of ΔG°_{ads} lower than -20 kJ mol^{-1}, are consistent with the electrostatic interaction between charged molecules and the charged metal surface (physisorption); those around -40 kJ mol^{-1} involve charge sharing or charge transfer from inhibitor molecules to the metal surface to form a coordinate type of metal bond (chemisorption) [33]. The calculated ΔG°_{ads} values of **1a**–**1d** are -33.33 to -35.46 kJ mol^{-1}, indicating their adsorption mechanism on carbon steel are both physisorption and chemisorption (Table 2). The large negative value of ΔG°_{ads} for **1c** shows its strong adsorption on the carbon steel surface. This isotherm assumes that the adsorbed molecules occupy only one site and there are no interactions with other adsorbed species [32].

The inhibition efficiency of a compound depends on several factors, including the number of adsorption active centers, the mode of interaction with the metal surface, and molecular size. The active centers in the structure of **1a**–**1d** are sulfur atoms, nitrogen atoms, oxygen atoms, and two aromatic rings (Fig. 1). The presence of two methoxy groups in **1c** enhances the possible interaction between the π-electrons with the vacant *d*-orbitals of iron atoms.

Conclusion

In summary, the corrosion behavior of four aryl-triazino-benzimidazole-2-thiones were investigated on carbon steel in 2 M HCl solution using SECM and weight loss measurements. The results of SECM measurements and local ferrous ion concentrations confirm that inhibitors reduce corrosion current and form a uniform film on the carbon steel surface. The average currents obtained by SECM or local ferrous ion concentrations were used for comparison of the IE of the studied aryl-triazino-benzimidazole-2-thiones. The inhibition efficiency of aryl-triazino-

benzimidazole-2-thiones increases with an increase in concentration of inhibitors. All the compounds exhibited more than 89 % inhibition activity at a concentration of 100 mg L^{-1}. When the inhibition efficiency was more than 85 %, SECM and weight loss results were comparable. The adsorption of the compounds on the carbon steel surface obeys Langmuir's adsorption isotherm. The calculated ΔG°_{ads} values for **1a**–**1d** were −33.33 to −35.46 kJ mol^{-1}. The ΔG°_{ads} values revealed that the corrosion inhibition of **1a**–**1d** on the metal surface are due to the formation physisorption and chemisorptions adsorption films.

Acknowledgments The authors are grateful for financial support of the Research Institute of Petroleum Industry.

References

1. A.J. Bard, F.R. Fan, J. Kwak, O. Lev, Anal. Chem. **61**, 132–138 (1989)
2. A.L. Barker, M. Gonsalves, J.V. Macpherson, C.J. Slevin, P.R. Unwin, Anal. Chim. Acta **385**, 223–240 (1999)
3. S. Amemiya, A.J. Bard, F.-R.F. Fan, M.V. Mirkin, P.R. Unwin, Annu. Rev. Anal. Chem. **1**, 95–131 (2008)
4. J.L. Fernandez, A.J. Bard, Anal. Chem. **75**, 2967–2974 (2003)
5. P. Sun, F.O. Laforge, M.V. Mirkin, Phys. Chem. Chem. Phys. **9**, 802–823 (2007)
6. P. Sun, Z. Liu, H. Yu, M.V. Mirkin, Langmuir **24**, 9941–9944 (2008)
7. L. Niu, Y. Yin, W. Guo, M. Lu, R. Qin, S. Chen, J. Mater. Sci. **44**, 4511–4521 (2009)
8. K. Fushimi, K.A. Lill, H. Habazaki, Electrochim. Acta **52**, 4246–4253 (2007)
9. N. Esmaeili, J. Neshati, I. Yavari, J. Ind. Eng. Chem. **22**, 159–163 (2015)
10. A. Davoodi, J. Pan, C. Leygraf, S. Norgren, Electrochim. Acta **52**, 7697–7705 (2007)
11. S. González, J.J. Santana, Y. González-García, L. Fernández-Mérida, R.M. Souto, Corros. Sci. **53**, 1910–1915 (2011)
12. S.S. Jamali, S.E. Moulton, D.E. Tallman, M. Forsyth, J. Weber, A. Mirabedini, G.G. Wallace, J. Electroanal. Chem. **739**, 211–217 (2015)
13. A.J. Bard, M.V. Mirkin, *Scanning Electrochemical Microscopy*, 2nd edn. (CRC Press, Taylor & Francis Group, LLC, Boca Raton, London, 2012)
14. G. Wittstock, M. Burchardt, S.E. Pust, Y. Shen, C. Zhao, Angew. Chem. Int. Ed. **46**, 1584–1617 (2007)
15. M.V. Mirkin, B.R. Horrocks, Anal. Chim. Acta **406**, 119–146 (2000)
16. Y. Yin, L. Niu, M. Lu, W. Guo, S. Chen, Appl. Surf. Sci. **255**, 9193–9199 (2009)
17. E. Volker, C.G.L. Inchauspe, E.J. Calvo, Electrochem. Commun. **8**, 179–183 (2006)
18. B.T. Luong, A. Nishikata, T. Tsuru, B.T. Luong, A. Nishikata, T. Tsuru, Electrochemistry **71**, 555–561 (2003)
19. J. Izquierdo, L. Nagy, J.J. Santana, G. Nagy, R.M. Souto, Electrochim. Acta **58**, 707–716 (2011)
20. K. Fushimi, M. Seo, Electrochim. Acta **47**, 121–127 (2001)
21. A.C. Bastos, A.M. Simoes, S. González, Y. González-Garcia, R.M. Souto, Electrochem. Commun. **6**, 1212–1215 (2004)
22. J. Zhu, H. Bienayme (eds.), *Multicomponent Reactions* (Wiley, Weinheim, 2005)
23. P.T. Anastas, L.G. Heine, T.C. Williamson, *Green Chemical Syntheses and Processes* (American Chemical Society, Washington, DC, 2000)
24. R.C. Cioc, E. Ruijter, R.V.A. Orru, Green Chem. **16**, 2958–2975 (2014)
25. B. Ganem, Acc. Chem. Res. **42**, 463–472 (2009)
26. L.H. Choudhury, T. Parvin, Tetrahedron **67**, 8213–8570 (2011)
27. A. Bhatnagar, P.K. Sharma, N. Kumar, Int. J. Pharm. Tech. Res. **3**, 268–282 (2011)
28. E.P. Sascha, M. Wiebke, W. Gunther, Z. Phys. Chem. **222**, 1463–1517 (2008)
29. J. Izquierdo, J.J. Santana, S. Gonzalez, R.M. Souto, Electrochim. Acta **55**, 8791–8800 (2010)
30. Y. González-García, G.T. Burstein, S. González, R.M. Souto, Electrochem. Commun. **6**, 637–642 (2004)

31. A.J. Bard, L.R. Faulkner, *Electrochemical Methods: Fundamentals and Applications* (Wiley, New York, 2001)
32. G. Avci, Colloids Surf. A Physicochem. Eng. Asp. **317**, 730–736 (2008)
33. E. Kamis, F. Belluci, R.M. Latanision, E.S.H. El-Ashry, Corrosion **47**, 677–686 (1991)